

Performance Analysis of Different Frequency Estimation Methods in GNSS-RO Receivers with Open Loop Tracking

L. Mohammadi¹, Sh. Amiri^{2*}

Received: 2015/9/24 Accepted: 2015/11/22

Abstract

One of the main challenges in tracking radio occultation (RO) signals of open loop approach is the excess Doppler estimation accuracy in lower troposphere. Propagation of RO signals through the lower troposphere with severe refractivity gradient results in high phase acceleration and low signal to noise ratio (SNR) signal. Because of the high refractivity in the lower moist troposphere, the received RO signals by global navigation satellite system (GNSS) receivers can have large excess Doppler which may vary rapidly. Due to limitation on bandwidth and transmitted information to post processing, we can't use very high sampling rate at GNSS receivers at LEO satellite. Therefore, try to enhance the accuracy of the Doppler predicted models in the satellite makes the GNSS-RO receivers by using efficiently frequency estimation method at GNSS receivers. In this regard, we investigate the event of RO signal and then the various frequency estimation methods to improve the estimates of the Doppler frequency in post processing are evaluated. The various frequency estimation methods are investigated from performance and computational complexity perspective. Via simulation, the excess Doppler estimation accuracy in post processing for different frequency estimation methods are compared by its root mean squared error. Based on simulation results, it is seen that both ESPRIT and Jacobsen with Bias schemes have the better performance and the estimation error of them are less than that of other methods.

Keywords: Radio occultation, Frequency estimation, Lower troposphere.

Introduction

A. State of the Art

Atmospheric sounding by means of global navigation satellite system (GNSS) radio occultation (RO) may contribute to improving in numerical weather prediction and climate change studies. RO occurs when an onboard receiver of low earth orbit (LEO) spacecraft tracks a GNSS satellite as it sets or rises through earth's atmosphere. The recorded phase and amplitude of the radio waves during the occultation can be analyzed to determine neutral atmospheric parameters, including refractivity, density, pressure, temperature, and humidity, as well as ionospheric total electron content (TEC) and refractivity profiles [1].

In the GNSS-RO technique, very challenging conditions exist for signals passing through the Earth's lower troposphere. Traditionally, the modulated GNSS signals are tracked using a phase locked loop (PLL) that relies on a feedback process to keep the reference signal sufficiently close. These errors, in turn, cause significant number of cycle slips and amplitude suppression. In tracking of RO signal, another important parameter is phase acceleration which is derived from the signal's phase and represents the rate at which signal's phase changes. Kernal acceleration technique allows one to convert the phase and Doppler frequency changes into refractive attenuation variations. From such derived refractive attenuation and amplitude data one can estimate the integral absorption of radio waves [2]. The value of this parameter in the lower troposphere is more than 2 kHz/sec which causes the variation of signal to be very high. Since the signal is weak and high dynamics, PLL can not be useful. To tackle this issue, open loop (OL) tracking is introduced where at first implemented on SAC-C and later adapted on Constellation Observing System for Meteorology, Ionosphere, and Climate (COSMIC) [3]. This method relies on a priori models of atmospheric Doppler and delay to track the occulting GNSS signal.

1. PhD student at the Iranian research organization for science and technology, IROST, Tehran, Iran. mohamady@itrc.ac.ir.

2. Associate professor at the Iranian research organization for science and technology, IROST, Tehran, Iran. amiri@irost.org.

In fact, the high sampling rate of the raw measurement enables a monitoring of the high frequency fluctuations and improves the spatial resolution of the refractivity profile. However, high sampling rate would demand huge amounts of data and require intensive ground-based processing and additional cost. Therefore, due to the cost constraints and limitation on the amount of information sent to the post-processing, reducing the sampling rate is considered. For this reason, try to enhance the accuracy of the Doppler predicted models to reduce the sampling rate from 1000 Hz to 50 Hz [4]. However, in the next receiver to achieve higher resolution, sampling rate of 100 Hz is used. In tracking RO, using of efficient excess Doppler estimation methods is critical, in this regards, we propose methods of frequency estimation called Jacobsen, Jacobsen with Bias, Macleod, Quinn, Parabolic and ESPRIT to improve excess Doppler estimation.

B. Related Works

In [4] and [5], the authors obtained estimation of excess Doppler based on the variations of amplitude and phase of the received signal. To do this, the received information at GNSS receiver payload is sent to the ground station for these estimations which this procedure is called post processing. Propagation of RO signals through the moist troposphere results in multipath and strong fluctuation of the phase and amplitude. Therefore, tracking such signals by PLL may result in large deviation of the signal phase from the phase model, updated with the use of feedback from the received signal [5]. This, in turn, results in random and systematic error (bias) in the extracted phase and in the retrieved refractivity. Moreover, the PLL tracking of the multi tone RO signals is unstable. Analysis of Doppler frequency results in ± 50 kHz and ± 2 kHz geometric and atmosphere Doppler, respectively [4] and [5]. The instability of the PLL tracking in the troposphere motivated [4], [6] and [7] to consider the OL tracking. In terms of reproducing the temperature and moisture profile in the lowest 2.5 km, statistical analysis is performed on a large number of COSMIC profiles in a region surrounding Macquarie Island [8]. The principles of the OL tracking of RO signals outlined in that study, including estimates of the necessary filter bandwidth and sampling rate. In real time, a RO signal must be subject to down-conversion in receiver, by use of the pre-calculated

phase model, without a feedback from the received signal. The down-converted RO signal is low-pass filtered, sampled and transmitted to the ground for post processing. In previous related works, the sliding window method is used for estimation of Doppler frequency which is one of radio holographic (RH) methods.

RH methods to process RO data in atmospheric multipath zones are suggested to improve retrieval accuracy in the moist lower troposphere: back propagation (BP) [9] and [10], sliding spectral (SS) [4], canonical transform (CT) [11], [12], full spectrum inversion (FSI) [13], CT2 [14] and phase matching (PM) [15]. SS method takes into account the whole spectral content of the signals in the small aperture. Different frequency estimation methods such as multiple signal classification (MUSIC) technique was used to test SS method by processing 4 GPS/MET occultations [16]. By spectral analysis the contributions from components of surface reflections were detected in 20% to 30% of CHAMP (Challenging Minisatellite Payload) occultations. Sokolovskiy in [17] thoroughly investigated the bias induced by the noise in RH methods, and gave a physical explanation. However, false spectral maxima induced by the noise can often result in retrieval errors in SS method. Therefore, accuracy of frequency estimation is very important in SS and other methods.

In this regard, the best coarse frequency estimation of the signal is from the peak of the N point discrete Fourier transform (DFT) of the received signal. A N point DFT is typically calculated for a data length of N samples which gives a resolution of $\frac{2\pi}{N}$. For real time spectral analysis, a well-known computationally efficient method is the sliding DFT especially in the cases when a new DFT spectrum is needed every few samples. The sliding DFT is computationally efficient than the radix-2 Fast Fourier Transform (FFT). The sliding DFT performs a N point DFT within a sliding window of N samples. The window is then shifted by a sample for the next iteration and a new N point DFT is calculated which utilizes the old N point DFT values [18] and [19]. In [20], the authors investigate a simple DFT-based algorithm for the single tone frequency estimation. Although DFT is very effective and, in the case of FFT, fast enough to be applied in real-time applications, it may become very inaccurate at the non-coherent

sampling because of the spectral leakage phenomena [21]. In [21], the authors introduced a new set of unbiased analytical estimators for the frequency of a complex sinusoid and showed that the new estimators are more accurate than the previous estimators. Frequency estimators mainly include non-iterative IpDFT algorithms and iterative DFT-based algorithms [22]. In [22], the authors proposed an iterative, exponentially windowed algorithm. Generally, a two-stage search can be implemented to improve the frequency estimation. First, a coarse estimation is usually performed by an N-point FFT to locate the index of the largest magnitude. Secondly, a fine search is executed around the vicinity of the index. An efficient and low complexity frequency estimation method based on the DFT samples is described in [23]. The suggested method can operate with an arbitrary window function in the absence or presence of zero-padding. The frequency estimation performance of the suggested method is shown to follow the Cramer–Rao bound (CRB) closely without any error floor due to estimator bias, even at exceptionally high signal-to-noise-ratio (SNR) values.

There are many methods for estimation of the frequency of a signal. The estimation of the frequency of a signal has been dealt with extensively in the literature [24] and [25]. Most of the frequency estimation methods can be grouped into two classes [26] and [27]: parametric or high-resolution methods and non-parametric or periodogram-based methods. Non-parametric frequency estimation methods are based on the Fourier transform of the data sequence or its autocorrelation function. They do not require any knowledge of the data sequence.

These methods are straightforward to use and provide reasonably high resolution for sufficiently long data sequences. The FFT makes it convenient to calculate the periodogram spectral estimate or any of its variations [26] and [28]. Also, periodogram method have high variance, which does not decrease with increasing data length. Modified methods with lower variance have been developed, but with the cost of decreased resolution. They exploit averaging (Bartlett), windowing (Blackman-Tukey) or both (Welch) to lower the variance. All of these methods have more or less equal properties and performance for long data lengths. Hence, to increase frequency resolution, a longer measurement time must be

used. In order to achieve sub-Hertz resolution with the DFT, a measurement time of several seconds is required. Classical non-parametric spectral estimators are still the most robust for low SNR, but they can not exploit high SNR conditions [29]. In addition, these methods are applicable to all signal classes and the estimated power spectral density (PSD) is directly proportional to power. The main disadvantage of these methods is their low resolution limited by windowing effects. MUSIC and ESPRIT are high-resolution methods which are intended for estimating spectral lines (frequencies).

Signals in the fields of e.g., communications, radar, sonar, and geophysical seismology can be described with sinusoidal model [30]. These methods are based on an eigenvector decomposition of autocorrelation matrix of the data into two subspaces, one associated with the signal and the other associated with the noise. Eigenvalues relate to the noise variance and the methods utilize the orthogonality property between signal vectors and noise subspace eigenvectors. High-resolution subspace methods provide very accurate frequency estimates with only small differences in statistical performance and computational load. In addition, they are able to resolve more closely spaced spectral lines than classical methods. Note that the fundamental difference to classical methods is, that subspace methods are not based on the Fourier transform of the data sequence or its estimated correlation function [26]. ESPRIT has been developed primarily for spatial direction of arrival (DOA) estimation [29] and [31]. This method exploits invariance of two time displaced data sets to determine sinusoid frequencies, powers, and noise variance. The number of sinusoids must be known in advance and the algorithm tries to find this number of sinusoids, the strongest ones. The performance of ESPRIT is in most cases slightly better than the performance of MUSIC method. Moreover, it has lower computational cost and no problems in separating the signal roots from the noise roots [29]. The high-resolution methods are able to resolve spectral peaks separated in frequency less than $1/T$ (T being the observation time of the signal), which is the resolution limit for the methods based on the periodogram. This class methods such as the MUSIC method and more recently, the ESPRIT method [31] have been proposed in the literature [32], [33], [34], [35] and

[36]. Quinn [32] uses the complex Fourier coefficients in order to interpolate the true signal frequency between the maximum and the second highest bin. However, Quinn's algorithm has been shown to have a frequency dependent performance, [37]. Furthermore, it is highly desirable, in the context of digital signal processor (DSP) implementation, to avoid divisions and functions with long Taylor series expansions. Zakharov and Tozer [35, 18] present a simple fine search that relies only on real multiply and accumulate (MAC) operations to refine the frequency estimate. The resulting frequency algorithm, called the dichotomous search of the periodogram peak, is particularly suited for DSP implementation. Also, in comparison with Quinn's algorithm, it achieves the CRB uniformly in frequency. The same authors propose in [34] a number of hybrid estimators that combine the dichotomous search with various interpolation techniques in order to reduce the computational complexity. Aboutanios and Reisenfeld [36] follow similar concept by using Quinn's interpolation algorithm to initialize the dichotomous search algorithm. This reduces the number of iterations required for convergence while achieving the CRB. Based on the existing works, there is no related works on the excess Doppler estimation via frequency estimation methods called Jacobsen, Jacobsen with Bias, Macleod, Quinn, Parabolic and ESPRIT in RO system.

C. Our Contributions

In this paper, we study the potential benefits of various frequency estimation methods in the estimation of excess Doppler, with the goal of minimizing frequency estimation error. Besides, we compare the various frequency estimation methods in post-processing from computational complexity and performance. To the best of our knowledge, no work has investigated the various frequency estimation methods called Jacobsen, Jacobsen with Bias, Macleod, Quinn, Parabolic and ESPRIT in RO system. The goal of this paper is performance analysis of different frequency estimators in RO systems and the main results and original contributions of this paper are the following:

- We identify the challenges of estimating the frequency of RO signals and we propose a framework to study it.

- We introduce efficient frequency estimation methods for RO system.

- We Compare the performance of different proposed frequency estimation methods and provide the analytical results that show how precise/effective our introduced estimators are.

This paper is organized as follows. In Section II, we investigate RO signal processing by using OL tracking. Then, we investigate the various frequency estimation methods in Section III. The performance of different frequency estimation methods is studied in Section IV. Simulation results are presented in Section V, and conclusions are in Section VI.

RO Signal Processing by Using OL Tracking

In OL tracking, the signal is down-converted via a numerically controlled oscillator (NCO), which produces a frequency given by an onboard Doppler model pre-calculated in GNSS receiver without a feedback from received signal. Next, in order to remove the noise from data i.e., on amplitude and phase of signal, a zero-phase low-pass filter was adopted. The baseband signal is typically then sampled at a rate of 100 Hz.

For simplicity, we use global position system (GPS) satellite signal for numerical weather prediction and climate change studies. GPS satellites broadcast on three frequencies: $L1$ (1575.42 MHz), $L2$ (1227.60 MHz) and $L5$ (1176.45 MHz) signals. When GPS RO signals are used for monitoring the lower troposphere, the ionospheric effect has to be removed. Thus, GPS $L1$ signal is enough for the processing of RO. In this paper all calculations are provided for GPS $L1$ frequency, thus only processing of $L1$ signal will be discussed.

The signal must be down-converted in the receiver with the use of the frequency model, $f_{mod} = f_c + f_{dop}$, based on predicted GNSS and LEO orbits and refractivity climatology. An additional error in the frequency model f_{mod} is introduced by the receiver clock, Δf_{LEO} , which depends on the receiver clock stability and it is reduced in the recent missions by using more stable oscillators. Thus after the down-conversion the mean frequency of the RO signal is shifted from zero because of neutral atmospheric mismodeling, ionospheric mismodeling, receive clock error, and relativistic effects not modeled by the special GNSS carrier frequency shift. To minimize noise aliasing, it must be at first low-pass filtered with

100 Hz bandwidth, then sampled in phase and quadrature and down-linked to the ground [4] and [5].

The sampling rate generally has to be equal to the spectral bandwidth of the signal. However, since the spread part of the spectrum occupies only part of the full spectral band, the sampling rate may be lower. When the sampling rate is greater or equal to the full spectral bandwidth of the signal, that is, ~ 100 Hz, the spectrum is reproduced without aliasing and the signal may be completely recovered from its complex samples. Lower sampling rates may result in aliasing of harmonics in the signal spectrum. However, if the sampling rate is not less than the spread part of the spectrum (where most of the signal power is concentrated), that is, ~ 50 Hz, then aliasing will not result in overlapping of harmonics [4] and [5].

In this case, the signal can still be recovered from its samples with minimal errors after an additional down-converted which eliminates or substantially reduces the aliasing. If the sampling rate is smaller than the spread part of the spectrum, then the aliasing will lead to the overlapping of harmonics and the signal cannot be recovered without corruption [4] and [5].

In OL signal tracking mode, ultimately, the receiver NCO is not driven by the observations, but by an a-priori Doppler frequency model [4], [5] and [6]. Then, the down-converted signal is passed through the low pass filter. However, in [4], [5] and [6] noted that the modelling error is ± 25 Hz, which it is variable and depend to atmospheric Doppler model. In order to remove the navigation data modulation (NDM) and connect the phase, the sampled signal must be down-converted to shift its mean frequency as close to zero as possible. Then, in postprocessing, the received signal is down-converted by use of the more accurate phase model. The purpose of this down-conversion is to remove the NDM and connect the phase between samples. The NDM can be removed using by two methods (internal and external) [6]. After computing of amplitude and accumulated phase, we can obtain bending angle and impact parameter. Then, by using of Abel transform, the refractivity profile can be provided. Finally, the atmospheric parameters such as pressure, temperature and water vapor pressure can be extracted from the refractivity profile. In Fig. 1, block diagram of the RO data processing for OL tracking is shown.

Frequency Estimation Methods

Retrieval of atmospheric parameters from RO data often encounters difficulties in the moist lower troposphere. Under conditions of atmospheric multipath propagation, calculation of bending angle from Doppler frequency shift is usually not applicable. RH methods are suggested to improve retrieval accuracy in the moist lower troposphere. SS method uses spectral analysis of the received signals in small sliding apertures. As a function of the impact parameter, the bending angle is computed from the frequency of each spectral maximum and its corresponding position at the aperture center. Sorting out the doubtful maxima can improve accuracy of SS method, especially in the lower troposphere [38]. Therefore, high resolution excess Doppler estimation is important problem at postprocessing in the RO occultation system and especially in SS method.

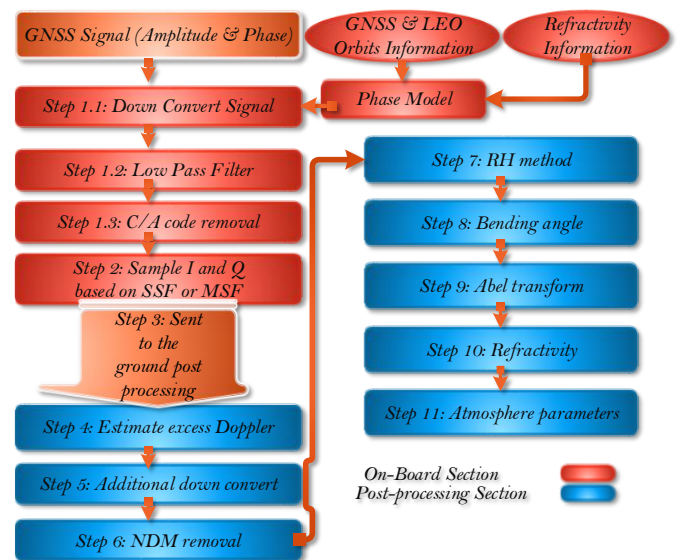


Fig 1. Block diagram of the RO data processing.

The high-resolution methods are able to resolve spectral peaks separated in frequency less than $1/T$ (T being the observation time of the signal), which is the resolution limit for the methods based on the periodogram. To this class pertain methods such as Pisarenko's method, the MUSIC and the Root-MUSIC, the Min-Norm method and more recently, the ESPRIT method [31]. All the high-resolution methods provide very accurate frequency estimates, with only small differences in their statistical properties. For our comparative

study, we have selected the ESPRIT method for two reasons: first, it provides slightly more accurate estimates than the other methods [26], and second, ESPRIT is not widely known to the vibration analysis community. In vibration analysis, long data records are typically acquired and therefore a simple FFT algorithm provides enough resolution for frequency estimation. Moreover, the requirement of real-time analysis is another reason that explains why classical frequency estimation methods such as the periodogram (probably windowed and averaged) still remain the most used tools in vibration analysis. However, as it is shown in [39], if a slight increase in the computational cost can be afforded, it is possible to obtain high-accuracy frequency estimates working with a relatively short data set. However, in general, periodogram or FFT-based methods cannot resolve closely spaced frequencies. Spectral analysis considers the problem of determining the spectral content (i.e., the distribution of power over frequency) of a time series from a finite set of measurements, by means of either nonparametric or parametric techniques [40]. Parametric methods may offer more accurate spectral estimates than the nonparametric ones. The parametric approach can thus be used only when there is enough information about the studied signal, that allows formulation of a model. Otherwise the nonparametric approach should be adopted. The parametric frequency estimation methods are frequency estimation techniques with high resolution. There have been several parametric frequency estimation methods such as: MUSIC, Root MUSIC, ESPRIT and Pisarenko [41]. The ESPRIT method is a parametric high-resolution technique. Note that the nonparametric methods of spectral estimation rely entirely on the definitions of PSD to provide spectral estimates. These methods constitute the "classical means" for PSD estimation. Nonparametric methods are based on the FFT. Spectral analysis of sampled signals is usually based on the DFT, which can be efficiently calculated with the FFT. Spectral analysis of sampled signals is usually based on the DFT, which can be efficiently calculated with the FFT. Although this approach is popular and suitable for a wide range of signals, it does not offer a good solution for the very accurate measurement of the frequency of individual sinusoids [42]. To begin with, the frequency resolution in Hertz is approximately the reciprocal of the measurement

interval in seconds. Secondly, spectral leakage of broadband noise and harmonic interference causes weak signals to be distorted and obscured [28]. These two performance limitations are particularly troublesome when analyzing short data records, which are present e.g. in radar and sonar. On the other hand, to achieve adequate frequency resolution in a navigation application, very long data records should be used, leading to prohibitive processing load and impractical memory requirements. One approach to deal with this problem is based on interpolation between the discrete points of a DFT spectrum, thus achieving sub-bin resolution for frequency and phase estimates. This is attained at a cost of increased processing load [42].

A single complex sinusoid with white Gaussian noise can be represented in the form

$$x[n] = A \exp(j\omega n) + w[n], \quad (1)$$

where A and ω are unknown variables which represent the amplitude and frequency of the complex sinusoid respectively where $\omega = \frac{2\pi(k_{peak} + \delta)}{N}$ and k_{peak} is the index of the peak of the sliding DFT. δ is to be estimated from the three samples around the peak of the sliding DFT where $|\delta| < 1/2$. The transfer function for N point sliding DFT filter can be represented as

$$H(z) = \frac{1 - r^N z^{-N}}{1 - r e^{\frac{j2k\pi}{N}} z^{-1}}, \quad |r| < 1. \quad (2)$$

where r is damping factor which can use to force the pole of filter to be at a radius of r inside the unit circle.

Therefore, a particular output bin of sliding DFT is written as

$$X_k = \sum_{n=0}^{N-1} x[n] r^n e^{-\frac{2kn\pi}{N}}, \quad |r| < 1 \quad (3)$$

In practice though a particular output bin can be found out using the following recursive relation which basically serves the computational efficiency purpose

$$X_k[n] = X_k[n-1] r e^{\frac{j2kn\pi}{N}} - x[n-N] r^N + x[n]. \quad (4)$$

The FFT-based methods combine techniques to reduce the effects of windowing with an iterative procedure which, at each iteration, detects the strongest peak and subtracts its effect (to reduce the interference resulting from spectral leakage). Doppler frequency estimate with high accuracy in post-processing is very important. As shown in Fig. 2, the idea is to estimate the frequency of the spectral peak k_{peak} based on three DFT samples: X_{k-1} , X_k , and X_{k+1} [41]. If we selected k_{peak} by making it equal to the k index of the largest DFT magnitude sample, then the maximum estimation error in k_{peak} would be equal to half the width of the DFT bin.

However, if it is adopted the frequency-domain peak sample X_k , and one or two adjacent samples, the estimate of the peak location could be more accurate if we it was used simple best or approximate-fit algorithms. In this section, we provide a fractional correction term δ to be added to the integer peak index k to determine a fine estimate of the spectral peak location k_{peak} located at the cyclic frequency f_{tone} .

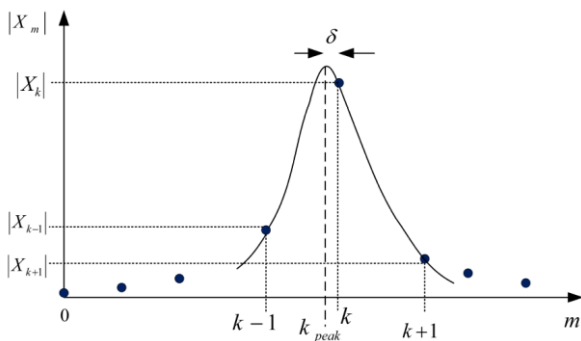


Fig 2. DFT magnitude samples of a spectral tone.

$$k_{peak} = k + \delta \quad (5)$$

$$f_{tone} = \frac{k_{peak} f_s}{N}, \quad (6)$$

where f_s is the time data sample rate in Hz and N is the DFT size. The sliding DFT bin where the peak occurs and its immediate neighbors can be represented as follows:

$$X_k = A \sum_{n=0}^{N-1} r^n e^{j2\pi/N\delta n} + W_k \quad (7)$$

$$= Af(\delta) + W_k,$$

$$X_{k-1} = A \sum_{n=0}^{N-1} r^n e^{\frac{j2\pi}{N(\delta+1)n}} + W_{k-1} \quad (8)$$

$$= Af(\delta + 1) + W_{k-1},$$

$$X_{k+1} = A \sum_{n=0}^{N-1} r^n e^{\frac{j2\pi}{N(\delta-1)n}} + W_{k+1} \quad (9)$$

$$= Af(\delta - 1) + W_{k+1},$$

where W_k is the DFT of $w[n]$ which also is white and

$$f(\alpha) = \sum_{n=0}^{N-1} r^n e^{j2\pi/N\alpha n}. \quad (10)$$

The aim is to estimate the value of δ from these three samples X_k , X_{k-1} and X_{k+1} so that $\hat{\omega} = 2\pi/N(k_{peak} + \delta)$ becomes the fine frequency estimate.

Many spectral peak location estimation solutions with different computational complexities have been described [32], [33], [37], [43], [44] and [45]. Here, we focus on six accurate and computationally simple, estimators. An example of a computationally simple peak location estimation that uses three DFT magnitude samples [46] and [47] makes use of a correction term given by

$$\delta = \frac{|X_{k+1}| - |X_{k-1}|}{4|X_k| - 2|X_{k+1}| - 2|X_{k-1}|} \quad (11)$$

The expression is simple, but it is statistically biased and performs poorly in the presence of noise. Some simple changes to (11) improve its accuracy dramatically [41], for instance by using the complex DFT values rather than the magnitudes as follows

$$\delta = \frac{|X_{k+1}| - |X_{k-1}|}{2|X_k| - |X_{k+1}| - |X_{k-1}|} \quad (12)$$

The accuracy of the spectral peak location estimation has been improved and the statistical bias of (11) has been eliminated. Even more, (12) provides potential for computation reduction by avoiding the nontrivial magnitude calculations in (11). While the solution in (12) works well when a rectangular time-domain window is applied to the DFT's input samples, it is often beneficial or necessary to use non-rectangular windowing. One

computationally simple alternative that is useful when time-domain data windowing has been used is given by [41]

$$\delta = \frac{P(|X_{k+1}| - |X_{k-1}|)}{|X_k| + |X_{k-1}| + |X_{k+1}|} \quad (13)$$

where the scaling constant P can be adjusted for different window functions [48]. However, (13) needs the computation of the DFT magnitude samples. Inspired by (12) and (13), a solution for use with non-rectangular windowed time samples has been suggested that does not require DFT magnitude computations; it is given by [41]

$$\delta = \frac{Q(|X_{k-1}| - |X_{k+1}|)}{2|X_k| + |X_{k-1}| + |X_{k+1}|} \quad (14)$$

where Q is a window-specific scaling constant [41] and [49].

The above methods can be used for all symmetric window functions. However, its estimation accuracy is related to window function. There is higher estimation precision with the Hanning window, while lower accuracy with the rectangular window. The window length must be short enough to provide an acceptable frequency accuracy. Moreover, by increasing in phase acceleration, to obtain acceptable frequency accuracy, the window length must be decreased. Since these methods are simple and quick, they are widely used in low noise environments. The disadvantage is that they need different analysis for different window functions [18]. In [50], the authors proposed parabolic interpolation algorithm to correct estimation error which is as follow

$$\delta = \frac{|X_{k+1}| - |X_{k-1}|}{4|X_k| - 2|X_{k-1}| - 2|X_{k+1}|} \quad (15)$$

In [37], Quinn introduced the following algorithm

$$\alpha_1 = \Re(X_{k-1}/X_k), \quad (16)$$

$$\alpha_2 = \Re(X_{k+1}/X_k), \quad (17)$$

$$\delta_1 = \frac{\alpha_1}{1 - \alpha_1}, \quad (18)$$

$$\delta_2 = \frac{\alpha_2}{1 - \alpha_2}, \quad (19)$$

$$\text{If } \delta_1 > 0 \text{ and } \delta_2 > 0, \hat{\delta} = \delta_2 \text{ else } \hat{\delta} = \delta_1. \quad (20)$$

In [33], Macleod proposed the following algorithm

$$d = \frac{\Re\{X_{k-1}X_k^* - X_{k+1}X_k^*\}}{\Re\{2|X_k|^2 + X_{k-1}X_k^* + X_{k+1}X_k^*\}}, \quad (21)$$

$$\delta = \frac{\sqrt{1 + 8d^2} - 1}{4d}. \quad (22)$$

In [41], Jacobsen developed an estimation method that uses of a correction term given by

$$\delta = \Re\left\{\frac{X_{k-1} - X_{k+1}}{2X_k - X_{k-1} - X_{k+1}}\right\}, \quad (23)$$

Previous correction terms are effective for high SNR values, but it comes at almost no additional computational cost and therefore can be used at any SNR level. In the high SNR values, previous correction term have bias, therefore, the correction bias algorithm is proposed as follow [51]

$$\hat{\delta} = \frac{\tan(\pi/N)}{\pi/N} \Re\left\{\frac{X_{k-1} - X_{k+1}}{2X_k - X_{k-1} - X_{k+1}}\right\}, \quad (24)$$

It is well known that when the observation noise is white and Gaussian, the maximum likelihood frequency estimate of a single complex exponential waveform is the peak location of the discrete-time Fourier transform (DTFT) of the received signal. Since DTFT computation over the continuum of $[0, 2\pi]$ is a formidable operation, the samples of the DTFT are calculated using the DFT. Typically an N -point DFT is calculated for the data length of N samples leading to a resolution of $2\pi/N$ on the frequency estimate. In many applications, it is desirable to increase the resolution of the frequency estimate at the cost of some additional computation. As described in [52], a two-stage search can be implemented to improve the frequency estimate. First a coarse search with an N -point DFT is executed and then a fine search is implemented around the vicinity of the peak determined in the first stage. It should be noted that the resolution of a two-stage search is limited to the spacing of the grid points used in fine search. In [32], [33], [37] and [53] an alternative for the second stage is suggested. Instead of a grid search, the fine resolution estimate is produced through a function on DFT samples already calculated in the first stage. The methods suggested in [32], [33] and [37], use three DFT samples, while the method of Provencher uses

only two DFT samples, [53]. These methods require very few operations compared with the grid search and produce a real valued estimate for the frequency, instead of a discrete grid point. In [32], Jacobsen has suggested a simple relation for DFT domain fine frequency estimation. The suggestion is based on empirical observations and presented without a proof. In [51], the authors proposed a derivation for the Jacobsen formula and present a bias correction. The correction term is effective for high SNR values, but it comes at almost no additional computational cost and thus can be used at any SNR level. Note that the ESPRIT algorithm was proposed to estimate the frequencies of a set of complex exponentials in noise and it was further developed in the context of array signal processing [31] and [54]. Here, we briefly summarize its main characteristics. Without loss of generality, let us consider a signal composed of P sinusoids corrupted by noise,

$$x[n] = \sum_{i=1}^P A_i \cos(2\pi f_i n + \theta_i) + w[n], n = 0, \dots, N - 1 \quad (25)$$

where $w[n]$ is a white Gaussian noise of power σ^2 . Assuming that the phases are random with uniform distribution, the autocorrelation of $x[n]$ is given by

$$R_x[m] = \mathbb{E}\{x[n]x[n+m]\} + \sum_{i=1}^P \frac{A_i}{2} \cos(2\pi f_i m) + \sigma^2 \delta[m], \quad (26)$$

where $\delta[m] = 1$ if $m = 0$, and 0 otherwise. Using this model, the $(M \times M)$ (we assume that $2p < M < N$) data covariance matrix is given by

$$\mathbf{R} = \begin{pmatrix} R_x[0] & R_x[1] & \dots & R_x[M-1] \\ R_x[1] & R_x[0] & \dots & R_x[M-2] \\ \vdots & \vdots & \ddots & \vdots \\ R_x[M-1] & R_x[M-2] & \dots & R_x[0] \end{pmatrix}, \quad (27)$$

which can be rewritten as

$$\mathbf{R} = \mathbf{A}\mathbf{P}\mathbf{A}^H + \sigma^2 \mathbf{I}, \quad (28)$$

where H denotes conjugate and transpose, \mathbf{I} is the $(M \times M)$ identity matrix and \mathbf{P} is the following $(2p \times 2p)$ diagonal matrix:

$$\mathbf{P} = \text{diag}\left(\frac{A_1^2}{2}, \dots, \frac{A_p^2}{2}, \frac{A_p^2}{2}, \dots, \frac{A_1^2}{2}\right). \quad (29)$$

Finally, by defining

$$a(f) = [1e^{-j2\pi f} \dots e^{-j(M-1)2\pi f}]^T (M \times 1). \quad (30)$$

The matrix \mathbf{A} is given by

$$\mathbf{A} = [a(f_1), \dots, a(f_p), a(-f_p), \dots, a(f_1)]^T (M \times 2p). \quad (31)$$

Analogous to other high-resolution algorithms, ESPRIT relies on properties of the data covariance matrix (27). Specifically, performing the singular-value decomposition of \mathbf{R} , we can write

$$\mathbf{R} = \mathbf{U}\mathbf{\Lambda}\mathbf{U}^H, \quad (32)$$

where $\mathbf{\Lambda}$ is a diagonal matrix with real eigenvalues ordered such that $\lambda_1 \geq \lambda_2 \geq \dots \geq \lambda_M > 0$. Note that the matrix $\mathbf{A}\mathbf{P}\mathbf{A}^H$ in equation (25) is rank-deficient: $\text{rank}(\mathbf{A}\mathbf{P}\mathbf{A}^H) = 2p < M$. This property allows to partition the eigenvalues/eigenvectors pairs into noise eigenvectors, corresponding to eigenvalues $\lambda_{2p+1} = \dots = \lambda_M = \sigma^2$; and signal eigenvectors corresponding to eigenvalues $\lambda_1 \geq \dots \geq \lambda_{2p} > \sigma^2$. Hence, we can decompose \mathbf{R} as

$$\mathbf{R} = \mathbf{U}_s \mathbf{\Lambda}_s \mathbf{U}_s^H + \mathbf{U}_n \mathbf{\Lambda}_n \mathbf{U}_n^H, \quad (33)$$

It can be shown that the matrix \mathbf{U}_s , which consists of the signal eigenvectors, can be written as [54]

$$\mathbf{U}_s = \mathbf{A}\mathbf{T}, \quad (34)$$

where \mathbf{T} is a full-rank matrix. This means that \mathbf{A} and \mathbf{U}_s span the same subspace. Unlike other subspace-based approaches, ESPRIT exploits the special structure of matrices \mathbf{A} and \mathbf{U}_s . In particular, \mathbf{A} can be partitioned into sub-matrices \mathbf{A}_1 and \mathbf{A}_2 as follows:

$$\mathbf{A} = \begin{bmatrix} \mathbf{A}_1 \\ \text{last row} \end{bmatrix} = \begin{bmatrix} \text{first row} \\ \mathbf{A}_2 \end{bmatrix}. \quad (35)$$

By the structure of \mathbf{A} (denoted as shift-structure), \mathbf{A}_1 and \mathbf{A}_2 are related by

$$\mathbf{A}_2 = \mathbf{A}_1 \Phi, \quad (36)$$

where Φ is a diagonal matrix with elements $e^{j2\pi f_i}$, $i = 1, 2, \dots, P$; on the diagonal. In this way, the frequency estimation problem reduces to that of estimating Φ . Similarly to \mathbf{A} , the matrix \mathbf{U}_s can be partitioned into sub-matrices \mathbf{U}_1 and \mathbf{U}_2 . Now, combining (36) and (34) we have

$$\mathbf{U}_2 = \mathbf{U}_1 \Psi, \quad (37)$$

where Ψ is related to Φ by

$$\Psi = \mathbf{T}^{-1} \Phi \mathbf{T}. \quad (38)$$

Since (38) is a similarity transformation, both Ψ and Φ have the same eigenvalues, from which we can obtain the estimated frequencies. Since in practice \mathbf{U}_1 and \mathbf{U}_2 are noisy estimates, the matrix Ψ is estimated in (37) by applying a total-least-squares (TLS) algorithm [55]. Similar to the other frequency estimation methods considered in this paper, here we assume that the number of sinusoids is known; thus, the only parameter to be selected is the order M of the matrix \mathbf{R} . If we want to estimate p real sinusoids the lowest value for M is $2p$, higher values for M will increase significantly the performance of the method. However, M cannot be increased too much since the computational burden grows as M^3 . Finally, the ESPRIT algorithm can be summarized as follows [55]:

1. Compute the eigen decomposition of the data covariance matrix of order MR .
2. Form \mathbf{U}_s by selecting the $2p$ eigenvectors corresponding to the largest eigenvalues.
3. Partition \mathbf{U}_s into \mathbf{U}_1 and \mathbf{U}_2 by deleting the last row and the first row as in (35).
4. Estimate $\hat{\Psi}$ by solving $\mathbf{U}_2 = \mathbf{U}_1 \Psi$ in a TLS sense.
5. Estimate the frequencies \hat{f}_i as $-\arg(v_i)/2\pi$, where v_i , $i = 2, 4, 2, \dots, 2p$, are the eigenvalues of $\hat{\Psi}$.

Comparison of Methods

In applications, implementation complexity is often an important issue. We calculate the number of operations, in terms of additions and multiplications. FFT-based algorithms to obtain accurate frequency, use three samples around the peak in the FFT spectrum. Therefore, computational complexity of FFT-based algorithms have the order of $O(N \log_2(N))$ operations, where N is the number of FFT points. In the simulation, N is set to 4. Computing the ESPRIT algorithm would require the order of $O(N^3)$ operations. Therefore, for higher number of N , the ESPRIT algorithm has higher computational complexity than that of FFT-based algorithms. Due to high variation signal phase and frequency in the troposphere layer, we can set lower values for N such as 4 and 8. Therefore, in the lower value of N , the computational complexity of two algorithms are low and the computational complexity doesn't restrict us for choosing frequency estimation algorithm. In addition to the computational complexity criteria, there are other three important criterions, called real time, accuracy and anti-noise ability, which can be considered for evaluating the proposed frequency estimation methods. To fulfill the instantaneous requirements, the proposed methods should be simple in principle and easy to be implemented. Moreover, based on the requirement of accuracy, the proposed methods can reach Cramer-Rao low bound and achieve unbiased estimation. Finally, according to the requirement of anti-noise ability, the algorithm is not easily impacted on noise, especially under the low SNR. We provide a compact summary of the frequency estimation methods. The Table.I demonstrates behavior of frequency estimation methods, for real-time, anti-noise capability, computational complexity, estimation accuracy and number of samples comparisons.

Table I. The Comparison Of Each Frequency Estimation Methods.

Method	Real-time	Anti-noise capability	Computational complexity	Estimation accuracy	Number of samples
Jacobsen	Good	Moderate	$O(N \log_2(N))$	Moderate	40× 100
Jacobsen with Bias	Good	Good	$O(N \log_2(N))$	Good	40× 100
Macleod	Good	Moderate	$O(N \log_2(N))$	Moderate	40× 100
Quinn	Good	Bad	$O(N \log_2(N))$	Bad	40× 100
Parabolic	Good	Bad	$O(N \log_2(N))$	Bad	40× 100
ESPRIT	Bad	Good	$O(N^3)$	Good	40× 100

Simulation Results

In this section, the performance of the proposed frequency estimation schemes are studied via computer simulation. Moreover, we present some simulation results to compare the performance of the six frequency estimation methods. We model the GNSS receiver's input as the sum of simulated signal and white Gaussian noise. In our simulation runs, SNR for strong and weak signals are equal to 20 dB and -10 dB, respectively. We choose sampling frequency rate, 100 Hz in the GNSS receiver. Furthermore, the length of the window and occultation time duration are $N = 4$ and $T = 40$ second, respectively. Sampling of 40 second duration signal by 100 Hz sampling rate results in $40 \times 100 = 4000$ samples. The root mean square error (RMSE) criteria is chosen to evaluate the proposed algorithms performance. The adopted RMSE with S trials for each experiment is defined as follows

$$RMSE[f(i)] = \sqrt{\frac{1}{S} \sum_{j=1}^S [|\hat{f}_{ij} - f_i|^2]} \quad (39)$$

where \hat{f} and f are the estimated and real frequency, respectively. Note that all results provided are averages of 1000 independent runs.

A. Effect of SNR on the excess Doppler Estimation Error

Here, we illustrate the effect of different values of SNR on the excess Doppler estimation error for proposed frequency estimation schemes. We choose phase acceleration equal to 1829 Hz/s and sampling frequency rate, 100 Hz in the proposed algorithms. Fig.3 shows the RMSE vs the SNR for the six frequency estimation methods (Jacobsen, Jacobsen with Bias, Macleod, Quinn, Parabolic, ESPRIT). As can be seen, by increasing the SNR, the excess Doppler estimation error for all frequency estimation methods is decreased. Esprit and Jacobsen with bias methods have better performance than that of other methods. As shown in Fig. 3, the Esprit method mainly has the same accuracy with Jacobsen with bias method. In low SNR, both Parabolic and Quinn methods aren't robust to noise. Thus, these methods have higher frequency estimation error than the other methods.

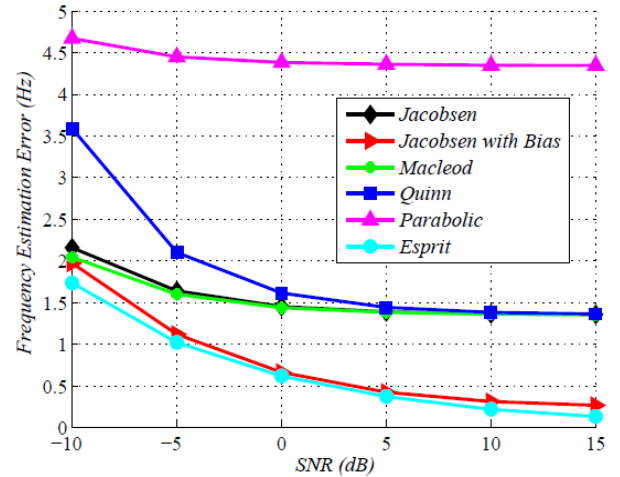


Fig 3. Excess Doppler estimation error versus SNR for different estimation algorithms. System parameters: phase acceleration is 1829 Hz/s and sampling frequency rate is 100 Hz.

B. Effect of Phase Acceleration on the excess Doppler Estimation Error

Here, we illustrate the effect of phase acceleration on the excess Doppler estimation error for different estimation algorithms. For simulation, the SNR is set between -10 dB and 20 dB and the frequency sampling is 100 Hz. Fig. 4 shows the RMSE versus the phase acceleration for the six frequency estimation methods (Jacobsen, Jacobsen with Bias, Macleod, Quinn, Parabolic, ESPRIT). It also shows that using the Esprit and Jacobsen with Bias estimation methods lead to an improved accuracy. However, by increasing phase acceleration value, the RMSE value is also increased. As shown in Fig. 4, there is smooth curve at phase acceleration below 2500 Hz/s. From 2500 Hz/s to 3000 Hz/s, due to the fast acceleration of phase, the frequency estimation methods do not follow any frequency change correctly. Therefore, the RMSE value increase sharply with the increasing of phase acceleration value.

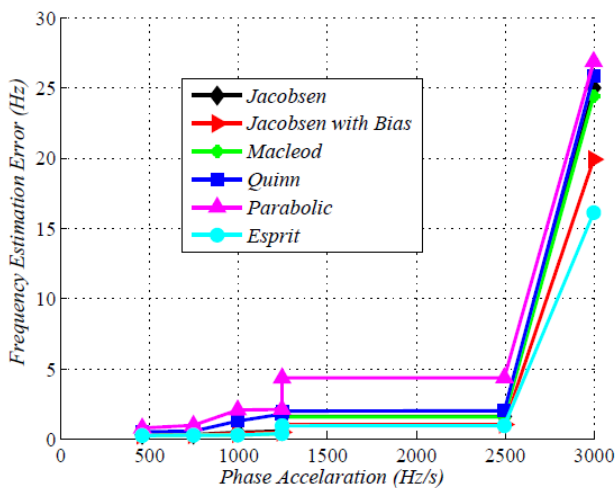


Fig 4. Excess Doppler estimation error versus phase acceleration for different estimation algorithms. System parameters: SNR is uniform distributed random variable between -10 dB and 20 dB and sampling frequency rate is 100 Hz.

Summary and Conclusions

Atmospheric sounding by means of GNSS-RO may contribute to improvements in numerical weather prediction and climate change studies. In other words, the goal of RO systems is to provide excess Doppler profile as a function of time, to anchor the variational bias correction of the climate and weather prediction data, and to provide better long-term consistency of the climate and weather analysis. Therefore, the accuracy of estimated excess Doppler in RO signal processing methods such as SS method is very important to reach this goal and better accuracy for weather prediction. Propagation of RO signals through the lower troposphere results in significant spreading of the signal spectrum. For this reason, OL tracking which tracks large random troposphere induced phase acceleration more reliably than PLL has to be applied. One of the challenges in tracking radio occultation signals of OL approach is the excess Doppler estimation accuracy. In order to properly estimate the frequency of a signal, the efficient frequency estimation methods must be used to the excess Doppler estimation in the post-processing. In this regards, in this paper, we investigated six different high-accuracy frequency estimation methods: Jacobsen, Jacobsen with Bias, Macleod, Quinn, Parabolic and ESPRIT were compared by each other from performance and computational complexity perspective. Based on the simulation results, ESPRIT scheme provides better results than that of other methods. Besides,

using simulation results, we showed that when the phase acceleration is increased very high and SNR is decreased, both ESPRIT and Jacobsen with Bias schemes have better performance than that of other schemes. In this situation, the ESPRIT scheme should be applied since it has the better performance.

References

- [1] W. H. Bai, Y. Q. Sun, Q. F. Du, G. L. Yang, Z. D. Yang, P. Zhang, Y. M. Bi, X. Y. Wang, C. Cheng and Y. Han, "An introduction to the fy3 gnos instrument and mountain-top tests," *Atmos. Meas. Tech.*, vol. 7, p. 1817–1823, June 2014.
- [2] A. G. Pavelyev, Y. A. Liou, J. Wickert, T. Schmidt and A. A. Pavelyev, "Phase acceleration: a new important parameter in gps occultation technology," *GPS Solutions*, vol. 14, no. 1, p. 3–11, May 2010.
- [3] C. O. Ao, G. A. Hajj, T. K. Meehan, D. Dong, B. A. Iijima, A. J. Mannucci and E. R. Kursinski, "Rising and setting GPS occultations by use of open-loop tracking," *Journal of Geophysical Research: Atmospheres*, vol. 114, no. D4, February 2009.
- [4] S. Sokolovskiy, "Tracking tropospheric radio occultation signals from low earth orbit," *Radio Science*, vol. 36, no. 3, p. 483–498, June 2001.
- [5] S. V. Sokolovskiy, "Nonlinear resonant circuit devices," *U.S. Patent 6,731,906 B2*, May 2004.
- [6] S. Sokolovskiy, C. Rocken, W. Schreiner, D. Hunt and J. Johnson, "Postprocessing of 11 gps radio occultation signals recorded in open-loop mode," *Radio science*, vol. 44, p. 1–13, May 2009.
- [7] S. Sokolovskiy, C. Rocken, D. Hunt, W. Schreiner, J. Johnson and D. Masters, "Gps profiling of the troposphere from space: Inversion and demodulation of the open-loop radio occultation signals," *Geophysical Research Letters*, vol. 33, no. 3, p. 483–498, April 2006.
- [8] L. B. Hande, S. T. Siems, M. J. Manton and D. H. Lenschow, "An evaluation of COSMIC radio occultation data in the lower atmosphere over the Southern Ocean," *Atmos. Meas. Tech.*, vol. 8, no. 1, pp. 97–107, Jan 2015.
- [9] M. E. Gorbunov, "Radio-holographic analysis of microlab-1 radio occultation data in the lower troposphere," *J. Geophys. Res.*, vol. 107, no. D12, 2002.
- [10] E. R. Kursinski, G. A. Hajj, S. S. Leroy and B. Herman, "The gps radio occultation technique,"

- Terr. Atmos. Oceanic Sci.*, vol. 11, no. 1, p. 53–114, 2000.
- [11] M. E. Gorbunov, "Canonical transform method for processing radio occultation data in the lower troposphere," *Radio Sci.*, vol. 37, no. 5, 2002.
- [12] M. E. Gorbunov and L. Kornblueh, "Analysis and validation of gps/met radio occultation data," *J. Geophys. Res.*, vol. 106, no. D15, p. 161–169, 2001.
- [13] A. S. Nielsen, "A. S. Jensen, M. S. Lohmann, H. H. BenFull spectrum inversion of radio occultation signals," *Radio Sci.*, vol. 38, no. 3, 2003.
- [14] M. E. Gorbunov and L. Kornblueh, "Analysis of wave fields by fourier integral operators and their application for radio occultations," *J. Geophys. Res.*, vol. 39, 2004.
- [15] A. S. Jensen, M. S. Lohmann, H. H. Benzon and A. S. Nielsen, "Geometrical optics phase matching of radio occultation signals," *Radio Sci.*, vol. 39, 2004.
- [16] K. Hocke, A. G. Pavelyev, O. I. Yakovlev, L. Barthes and N. Jakowski, "Radio occultation data analysis by the radio holographic method," *J. Atmos. Sol-Terr. Phys.*, vol. 61, p. 1169–1177, 1999.
- [17] S. Sokolovskiy, C. Rocken, W. Schreiner and D. Hunt, "On the uncertainty of radio occultation inversions in the lower troposphere," *J. Geophys. Res.*, 2010.
- [18] Q. Shuren and S. D. Huming, "Overview of correction methods for discrete spectrum," *Journal of vibration and shock*, vol. 26, no. 11, p. 138–145, May 2007.
- [19] D. Kang, "Accuracy analysis and improvement on center of gravity method for discrete spectrum frequency correction," *Journal of mechanical engineering*, vol. 46, no. 5, p. 43–48, May 2010.
- [20] X. Liu¹, Y. Ren, C. Chu and W. Fang, "Accurate Frequency Estimation Based on Three Parameter Sine-fitting With Three FFT Samples", *Metrology And Measurement Systems*, vol. XXII, no. 3, p. 403–416, 2015.
- [21] J. Liao and S. Lo, "Analytical solutions for frequency estimators by interpolation of DFT coefficients," *Signal Processing*, vol. 100, p. 93–100, 2014.
- [22] A. E. and S. Ye, "Efficient Iterative Estimation of the Parameters of a Damped Complex Exponential in Noise," *IEEE Signal Processing Letters*, vol. 21, no. 8, p. 975–979, 2014.
- [23] C. Candan, "Fine resolution frequency estimation from three DFT samples: Case of windowed data," *Signal Processing*, vol. 144, p. 245–250, 2015.
- [24] B. Boashash, "Estimating and interpreting the instantaneous frequency of a signal. i. fundamentals," in *Proceedings IEEE*, April 1992.
- [25] B. Boashash, "Estimating and interpreting the instantaneous frequency of a signal. ii. algorithms and applications," in *Proceedings IEEE*, April 1992.
- [26] P. Stoica and R. L. Moses, "Introduction to Spectral Analysis," *Upper Saddle River, NJ: Prentice-Hall*, 1997.
- [27] S. M. Kay, *Modern Spectral Estimation, theory and Application*, Prentice Hall, 1988.
- [28] S. M. Kay and S. L. Marple, "Spectrum analysis a modern perspective," in *Proceedings of the IEEE*, November 1981.
- [29] J. S. L. Marple, "Digital signal analysis," *CEI-Europe, Finspong, Sweden*, p. 512, March 1999.
- [30] C. W. Therrien, *Discrete Random Signals and Statistical Signal Processing*, Prentice Hall, Englewood Cliffs, NJ, 1992..
- [31] R. Roy and T. Kailath, " "Esprit estimation of signal parameters via rotational invariance techniques," *IEEE Transactions on acoustics, speech, and signal processing*, vol. 37, p. 984–995, July 1989.
- [32] B. Quinn, "Estimating frequency by interpolation using Fourier coefficients," *IEEE Transactions on Signal Processing*, vol. 42, no. 5, p. 1264–1268, May 1994.
- [33] M. Macleod, "Fast nearly ml estimation of the parameters of real or complex single tones or resolved multiple tones," *IEEE Transactions on Signal Processing*, vol. 46, no. 1, p. 141–148, January 1998.
- [34] Y. V. Zakharov, V. M. Baronkin and T. C. Tozer, "DFT-based frequency estimators with narrow acquisition range," in *Proc. Inst. Elect. Eng. Commun.*, 2001.
- [35] Y. V. Zakharov and T. C. Tozer, "Frequency estimator with dichotomous search of periodogram peak," *Electron. Lett.*, vol. 35, p. 1608–1609, 1999.
- [36] E. Aboutanios and S. Reisenfeld, "Frequency estimation and tracking for lowearth orbit satellites," in *Proc. 2001 Spring Vehicular Technology Conf.*, 2001.
- [37] B. Quinn, "Estimation of frequency, amplitude and phase from the DFT of a time series," *IEEE Transactions on Signal Processing*, vol. 45, no. 3, p. 814–817, March 1997.

- [38] M. E. Gorbunov, A. S. Gurvich and L. Kornbluh, "Comparative analysis of radioholographic methods of processing radio occultation data," *Radio Sci.*, vol. 34, no. 4, p. 1025–1034, 2000.
- [39] I. Santamaria, C. Pantaléon, J. Inabez and J. S. Iban Ez, "A Comparative Study Of High-Accuracy Frequency Estimation Methods," *Mechanical Systems and Signal Processing*, 2000.
- [40] P. Stoica and R. Moses, "Spectral analysis of signals", *Prentice hall*, 2004.
- [41] E. Jacobsen and P. Kootsookos, "Fast, accurate frequency estimators," *IEEE Signal Processing Magazine*, March 2007.
- [42] R. P. J. Schoukens and H. V. Hamme, "The interpolated fast fourier transform: A comparative study," *IEEE Transactions on Instrumentation and Measurement*, vol. 41, pp. 226-232, April 1992.
- [43] E. Jacobsen, "On Local Interpolation of DFT Outputs," [Online]. Available: Available online: <http://www.ericjacobsen.org/FTinterp.pdf> . [Accessed January 2013].
- [44] V. Jain, W. Collins and D. Davis, "High-accuracy analog measurements via interpolated FFT," *IEEE Transactions on Instrumentation and Measurement*, Vols. IM-28, p. 113–122, June 1979.
- [45] D. Rife and R. Boorstyn, "Single-tone parameter estimation from discrete-time observations," *IEEE Transactions on Information Theory*, Vols. IM-20, p. 591–598, September 1974.
- [46] V. Vetterling, W. Press, S. Teukolsky and B. Flannery, *Numerical Recipes in C*, Cambridge, United Kingdom: Cambridge Univ. Press, ch. 10., 1992.
- [47] P. Voglewede, "Parabola approximation for peak determination," *Global DSP Magazine*, vol. 3, no. 5, p. 13–17, May 2004.
- [48] K. Hawkes, "Bin interpolation," *Technically Speaking*, *ESL Inc. publication*, p. 17–30, January 1990.
- [49] R. Lyons, "Private communication," August 2006.
- [50] M. A. Richards, *Fundamentals of Radar Signal Processing*, New York: McGraw-Hill, 2005.
- [51] A. Candan, "A method for fine resolution frequency estimation from three DFT samples," *IEEE Signal processing letters*, vol. 18, no. 6, pp. 351–354, June 2011.
- [52] H. L. V. Trees, in *Detection, Estimation and Modulation Theory, Part.1*, New York, Wiley, 1971.
- [53] S. Provencher, "Estimation of complex single-tone parameters in the DFT domain," *IEEE Transactions on Signal Processing*, vol. 58, no. 7, p. 3879–3883, May 2010.
- [54] R. Roy, A. Paulraj and T. Kailath, "ESPRIT--A subspace rotation approach to estimation of parameters of cisoids in noise," *IEEE Transactions on Acoustics, Speech and Signal Processing*, vol. 34, no. 5, pp. 1340-1342, Oct 1986.
- [55] G. H. Golub and C. F. Vanloan, *Matrix Computations.*, Baltimore, MD: Johns Hopkins University Press, 1989.